Designing and Photophysical Properties of Optically Active Coacervate Droplets

M.Sc. Thesis

By

ABHISHEK ASHOK CHOURASIYA

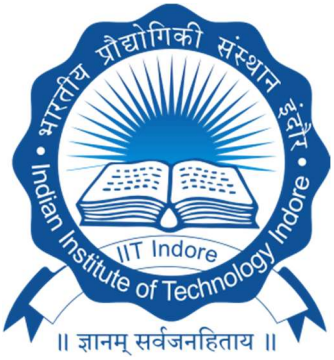

DEPARTMENT OF CHEMISTRY

INDIAN INSTITUTE OF TECHNOLOGY INDORE

May 2025

Designing and Photophysical Properties of Optically Active Coacervate Droplets

A THESIS

Submitted in partial fulfillment of the

requirements for the award of the degree

of

Master of Science

by

ABHISHEK ASHOK CHOURASIYA

DEPARTMENT OF CHEMISTRY

INDIAN INSTITUTE OF TECHNOLOGY INDORE

May 2025

INDIAN INSTITUTE OF TECHNOLOGY INDORE

CANDIDATE'S DECLARATION

I hereby certify that the work which is being presented in the thesis **Designing and Photophysical Properties of Optically Active Coacervate Droplet** in the partial fulfillment of the requirements for the award of the degree of **MASTER OF SCIENCE** and submitted in the **DEPARTMENT OF CHEMISTRY, Indian Institute of Technology Indore**, is an authentic record of my own work carried out during the time period from **July 2024** to **May 2025** under the supervision of Tushar Kanti Mukherjee, Professor, Discipline of Chemistry, IIT Indore. The matter presented in this thesis has not been submitted by me for the award of any other degree of this or any other institute.

Abhishek

Signature of the student

(ABHISHEK ASHOK CHOURASIYA)

This is to certify that the above statement made by the candidate is correct to the best of my/our knowledge.

Signature of Thesis Supervisor
(Prof. Tushar Kanti Mukherjee)

ABHISHEK ASHOK CHOURASIYA has successfully given his M.Sc. Oral Examination held on **15/05/2025.**

Signature of Supervisor of M.Sc. Thesis

Date: 20/05/2025

ACKNOWLEDGEMENTS

Initially, I express my gratitude towards my thesis supervisor, **Prof. Tushar Kanti Mukherjee**, for providing me with valuable guidance, suggestions, and supervision, as well as for offering constant encouragement throughout my research work.

Additionally, I express my gratitude to the members of my **PSPC**, **Dr. Pravarthana Dhanpal and Prof. Biswarup Pathak,** for their significant contributions and assistance. I am thankful to the **Department of Chemistry** at IIT Indore for providing me with the opportunity to undertake this research endeavor. Special acknowledgment goes to **Prof. Tushar Kanti Mukherjee**, the Head of the Department of Chemistry at the Indian Institute of Technology Indore, for his support and encouragement. I would also like to **thank Mr. Kinny Pandey, Mr Ghanshyam Bhavsar, Mr. Ravinder Kumar, Mr. Manish Kushwaha, Ms. Vinita Kothari, and Mr. Rameshwar Dauhare** for their technical support. I would also like to thank **Ms. Anjali Bandiwadekar, Mr. Rajesh Kumar, Mr. Lala Ram Ahirwar** and other library staff for their constant help, whenever required. Further, I would like to acknowledge SIC, IIT Indore, for instrumentation facilities.I wish to express my gratitude to **Suhas S. Joshi**, Director, IIT Indore, for his continuous support in every aspect.I would like to extend my gratitude to my laboratory colleagues and senior **Dr. Shivendra Singh, Dr. Chinmaya K. Patel, Mr. Supritam Datta, Mr. Prince Yadav, Mr. Saurabh Gupta and Mr. Sumit Mohapatra,** who consistently provided me with valuable insights and unwavering support in pursuit of the project's objectives. The information that you generously imparted to me was greatly motivating, not only for the present undertaking but also for the broader realm of communication practice.

Most importantly, I want to express my gratitude to my sister **Ms. Priyanjana Chourasiya**, who has always supported me and never let me down throughout my life. Finally, I'd like to express my deepest appreciation to my parents **Mr. Ashok Chourasiya and Mrs. Meena Chourasiya,** for all their support and encouragement during the duration of this endeavour.

ABHISHEK ASHOK CHOURASIYA

Dedicated to

My Family…..

ABSTRACT

Coacervate droplets have tremendous importance in various fields. Here, we have investigated the synthesis, characterization, and functional applications of the distinct coacervate systems: ATP droplets, MSA-capped CdTe QD droplets, and CD droplets. Using spectroscopic techniques, including UV-visible spectroscopy and confocal laser scanning microscopy (CLSM), coupled with quantitative equilibrium partition coefficient (K) measurements, we demonstrated the spontaneous sequestration of pyranine, a photoacid, within all the droplet systems. Notably, pyranine exhibited varying partition coefficients: 7.58 ± 1.2 in ATP droplets, 56.32 ± 5.6 in QD droplets, and 14.8 ± 2.1 in CD droplets, with the highest values observed in QD droplets indicating superior sequestration efficiency. Furthermore, we demonstrated preferential sequestration of the anticancer drug-DOX in pyranine-loaded CD droplets with a partition coefficient of 2.56 ± 0.3. The carbon dot-based coacervates proved particularly advantageous for therapeutic applications due to their biocompatibility, low toxicity, and chemical inertness compared to the potentially toxic QD-based systems. The sequestration mechanism was attributed to the hydrophobic and electrostatic interactions between the guest molecules and droplet matrices, allowing for efficient drug loading without chemical modification of the carriers. The most significant finding was the photo-responsive assembly and disassembly of these coacervate droplets in the presence of pyranine, as characterized by CLSM. This light-triggered behaviour, combined with the differential sequestration capabilities across droplet systems, positions these materials as promising candidates for diverse biomedical applications, particularly targeted drug delivery to tumor cells. This work advances the fundamental understanding of stimuli-responsive coacervate systems while demonstrating their practical utility in controlled therapeutic release.

TABLE OF CONTENTS

LIST OF FIGURES

List of Schemes

ACRONYMS

LLPS	Liquid-liquid phase separation
MSA	Mercaptosuccinic acid
QDs	Quantum dots
CDs	Carbon dots
NDs	Nano droplets
CdTe	Cadmium telluride
PDADMAC	Poly (diallyldimethylammonium chloride)
PDT	Photo Dynamic Theory
ATP	Adenosine triphosphate
PAGs	Photoacid generators
mPAHs	Metastable photoacids
EA	Electron-accepting moiety
NuH	Weakly acidic nucleophilic moiety
DOX	Doxorubicin
FL	Fluorescence
UV	Ultraviolet spectroscopy
CLSM	Confocal Laser Scanning Microscopy
kDa	Kilo Dalton
DIC	Differential interference contrast
DADMAC	Diallyldimethylammonium chloride

Abbreviation

˚C	Degree Celsius
h	Hour
M	Molar
L	Liter
g	Gram
mg	Milligrams
μL	Microliter
μM	Micromolar
mM	Millimolar
nm	Nanometer
μm	Micrometer
ζ	Zeta potential
r.t	Room temperature
cm	Centimeter
λ	Wavelength
λ_{ex}	Excitation wavelength
λ_{em}	Emission wavelength
mL	Milliliter
K	Equilibrium Partition Coefficient

CHAPTER 1: INTRODUCTION

1.1 Aim of the Project:

The aim of this project is to design optically active coacervate droplets and thoroughly investigate their photo-responsive nature in the presence of photoacids and photobases. By designing these functional coacervate droplets, the project seeks to explore how light can be utilized as an external stimulus to control the assembly and disassembly processes of the droplets under physiological conditions. Incorporating photoacids and photobases is critical, as these components can alter their protonation states upon exposure to specific wavelengths of light, leading to significant changes in the droplet's behavior. This dynamic response is expected to facilitate the controlled release of encapsulated biomolecules or therapeutic agents, making it particularly relevant for applications in targeted drug delivery systems. The project aims to elucidate the mechanisms by which light exposure influences droplet stability and functionality, thereby advancing our understanding of how these systems can be engineered for biomedical applications. Ultimately, this research aspires to contribute to the development of innovative materials that can respond intelligently to external stimuli, paving the way for new strategies in drug delivery and other therapeutic interventions that require precise control over molecular interactions and release profiles. Through systematic experimentation and analysis, this project will provide valuable insights into the design principles of light-responsive coacervate systems, enhancing their potential for practical applications in biomedical and photocatalytic applications.

1.2 Coacervation:

Coacervation, a spontaneous liquid-liquid phase separation (LLPS) phenomenon driven by electrostatic interactions between oppositely charged polyelectrolytes in aqueous media, enables the formation of self-assembled, spherical coacervate droplets with liquid-like properties. This process has been effectively utilized to engineer functional nanomaterials. In a previous investigation, Mukherjee and their colleagues demonstrated that mixing negatively charged mercaptosuccinic acid (MSA)-capped cadmium telluride quantum dots (CdTe-QDs) with the cationic polymer poly(diallyldimethylammonium chloride) (PDADMAC) results in the spontaneous formation of stable coacervate droplets (Scheme 1.1).[1]

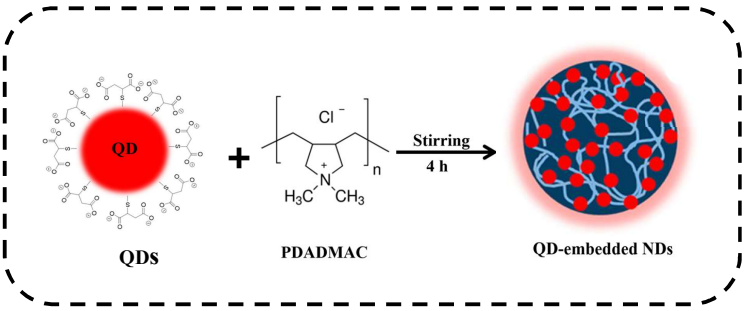

Scheme 1.1. Synthetic scheme of MSA- capped red QD-droplets.

Extending this methodology, CD-based nanodroplets can be synthesized by combining CDs with (PDADMAC), where the electrostatic attraction between the negatively charged CDs and the positively charged polymer drives self-assembly into nanostructured droplets (Scheme 1.2).[2] In both systems, i.e. CdTe-QDs and CDs, the interplay of electrostatic and hydrophobic interactions governs droplet stability and morphology, underscoring the versatility of coacervation for designing tailored nanocarriers. Such coacervate systems hold significant potential in applications ranging from drug delivery to catalytic platforms, as their composition and responsiveness can be modulated by adjusting polyelectrolyte ratios, pH, or ionic strength.

This approach not only highlights the fundamental principles of LLPS but also provides a scalable route for synthesizing advanced functional materials with precise control over their physicochemical properties

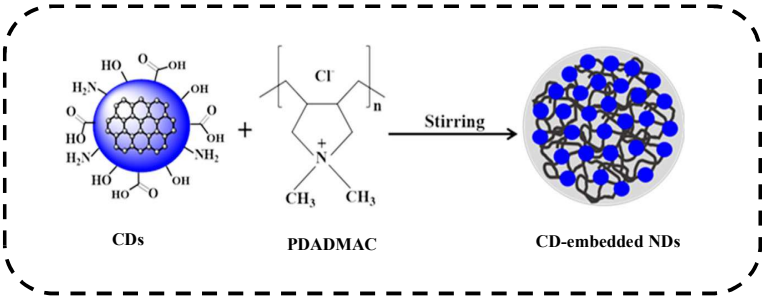

Scheme 1.2. Synthetic scheme of CD-embedded nano droplets

1.3 Light as an external stimulus:

Light-responsive systems are increasingly recognized for their significance in various applications, particularly in the assembly and disassembly of coacervate droplets. These systems utilize light as a non-invasive stimulus, allowing for precise control over droplet behaviour, which is crucial in fields such as drug delivery and biomolecular engineering. In the context of coacervate droplets, the incorporation of photoacids enhances their responsiveness to light. Upon exposure to specific wavelengths, photoacids can lead to an increase in proton concentration within the droplets, promoting their disassembly and facilitating the controlled release of encapsulated therapeutic agents at targeted sites. There are multiple benefits of using light as a stimulus. Light can be easily manipulated in terms of intensity, wavelength, and duration, providing researchers with the ability to fine-tune the timing and location of drug release. This capability is particularly advantageous in therapeutic applications where localized treatment is crucial, such as in cancer therapies that aim to minimize damage to surrounding healthy tissues. Previous research has demonstrated the effectiveness of light-responsive systems in achieving site-specific drug delivery, with studies highlighting their potential in (PDT), where light-sensitive compounds are used to target and destroy cancer cells upon

activation by specific wavelengths of light. Moreover, advancements in materials science have led to the development of hydrogels and polymeric systems that incorporate photosensitive moieties, enabling them to undergo structural changes upon light exposure, which can enhance their functionality in biomedical applications.[3] Overall, the integration of light-responsive mechanisms into coacervate droplets not only enhances their functionality but also opens up new avenues for innovative applications in biomedical fields, optical sensing, and these droplets, researchers can create advanced materials that respond dynamically to light stimuli, ultimately improving therapeutic outcomes and expanding the possibilities for targeted treatments.[4-5]

1.4 Quantum Dot:

QDs are semiconductor particles with nanoscale dimensions, typically ranging from 2 to 10 nm, that exhibit distinctive optical and electronic properties due to quantum confinement effects. Their emission colour varies depending on size; smaller quantum dots emit shorter wavelengths, such as violet to green, while larger quantum dots emit longer wavelengths, including yellow to red. This ability to tune emission wavelengths is a crucial characteristic that makes QDs valuable for applications in colour displays and lighting technologies. Additionally, QDs are known for their long photoluminescence lifetimes, allowing them to continue emitting light for extended periods after excitation, which enhances their utility in various fields, including bioimaging and optoelectronics.

Cadmium telluride (CdTe) QDs are particularly notable for their tunable band gap and high fluorescence efficiency. The optical properties of CdTe QDs can be significantly influenced by the choice of appropriate capping ligands, which stabilize the nanocrystals and affect their solubility and photoluminescence. Mercaptosuccinic acid (MSA) is one such ligand that enhances the stability of CdTe-QD, improving their fluorescence efficiency. MSA's structure, which includes two carboxyl groups, provides better stabilization. The use of different capping ligands allows for fine-tuning of the QDs surface

properties and enhances their performance in various applications, including targeted drug delivery and environmental sensing. Overall, the combination of CdTe QDs with appropriate capping ligands such as MSA enables the development of advanced materials with tailored characteristics for specific technological uses. In this project, I am dealing with MSA-capped CdTe red-emitting QDs (**Figure 1.1)**.

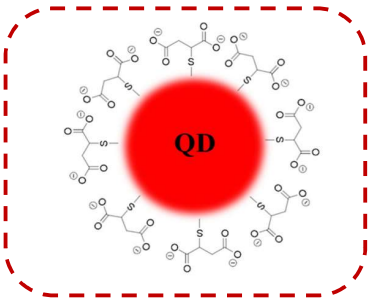

Figure 1.1. MSA-capped CdTe red QDs.

1.5 Carbon Dots:

Carbon dots (CDs) have emerged as a fascinating class of fluorescent nanomaterials. These nanoparticles, typically less than 10 nm in size, have garnered significant attention in the scientific community due to their unique properties and versatile applications. CDs are primarily composed of a carbonized core with surface functional groups. The core often consists of sp^2 and sp^3 hybridized carbon atoms, while the surface is rich in oxygen-containing groups such as carboxyl, hydroxyl, and carbonyl moieties. This structure contributes to their excellent water solubility and allows for easy surface functionalization. Among the various precursors used for CD synthesis, citric acid and ethylenediamine have gained particular prominence due to their ability to produce highly fluorescent CDs with excellent properties (Scheme 1.3). The observed ζ-potential of an aqueous dispersion of CDs is −31.3 ± 1.8 mV at pH 10, indicating the deprotonation of −OH and −COOH functional groups at the surface of CDs.[2] These CDs, typically produced through hydrothermal synthesis, exhibit remarkable photoluminescence. Their low cytotoxicity and biocompatibility make them ideal candidates for various biomedical

applications, including bioimaging, drug delivery, and sensing, over QD based droplets.

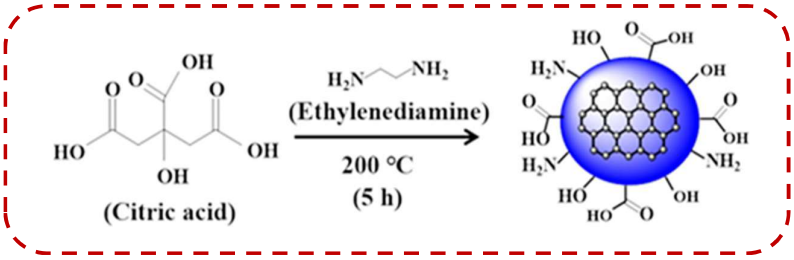

Scheme 1.3. Synthesis scheme of CDs.

1.6 (ATP) Adenosine triphosphate:

It is an essential molecule that is present in all living cells, functioning as the primary energy carrier. It's composed of three key parts: a nitrogenous base known as adenine, a ribose sugar, and a sequence of three phosphate groups **(Figure 1.2)**. ATP is crucial for various cellular processes, including muscle contraction, nerve signal transmission, and biochemical synthesis. When ATP interacts with poly(diallyldimethylammonium chloride) (PDADMAC), a positively charged polymer, it can lead to the formation of coacervate droplets. This process is known as coacervation, where oppositely charged molecules attract each other and spontaneously create liquid-like droplets. It was observed that ATP droplets are inhibited at pH values less than 3 and at high ionic strength.[6]

In this scenario, the negatively charged ATP molecules engage with the positively charged PDADMAC, resulting in the self-assembly of spherical coacervate droplets. These droplets have distinct properties due to their unique composition and structure. They can encapsulate a variety of biomolecules and serve as model systems for investigating membrane-less organelles and protocell behaviour. The interactions between ATP and PDADMAC are primarily driven by electrostatic forces, which help to stabilize these droplets in an aqueous environment.

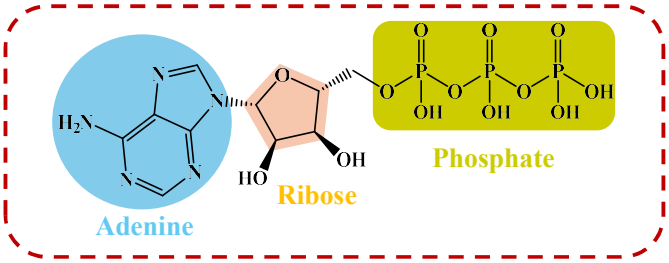

Figure 1.2. Adenosine 5′-triphosphate

1.7 PDADMAC:

Poly (diallyldimethylammonium chloride), also represented as PDADMAC, is a homopolymer of diallyldimethylammonium chloride (DADMAC). It is a cationic polyelectrolyte with high charge density. To synthesize monomer DADMAC, mix dimethylamine with allyl chloride (2-equivalent) (**Scheme 1**).[7] PDADMAC is synthesized by polymerization of DADMAC via a radical polymerization mechanism in the presence of organic peroxide as a catalyst **(Scheme 2)**.[8] During this polymerization two polymeric structures are possible: N-substituted pyrrolidine or N-substituted piperidine structure, out of those two the pyrrolidine structure is more favoured.

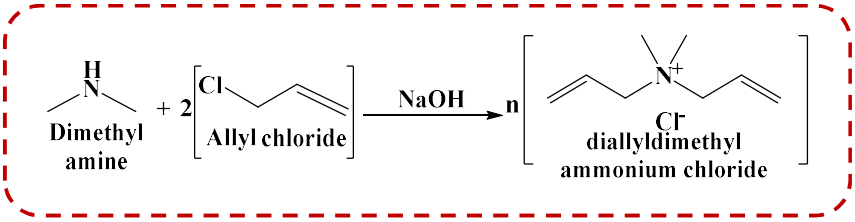

Scheme 1. Synthesis scheme of DADMAC

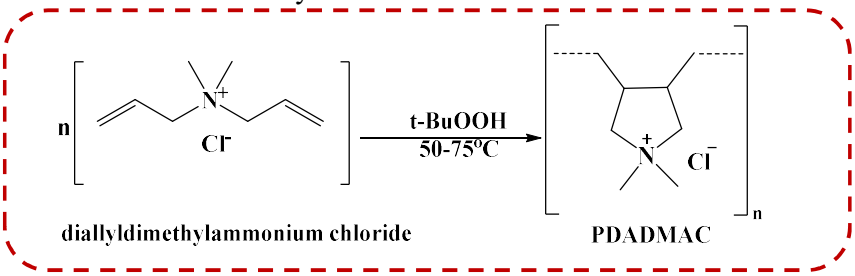

Scheme 2. Synthesis scheme for the Polymerization of DADMAC to Synthesize PDADMAC.

1.8 Photoacids:

A photoacid is a molecule that becomes a strong acid upon exposure to light thus linking photons to protons.[9-12] This feature makes it possible to control the processes of transfer of proton by light, which is crucial in many reactions, chemical and material as well as biological ones. This includes acid-catalyzed reactions, pH-sensitive materials. And so, we can say that photoacids enable the proton transfer without direct contact, offering a method to convert light energy into other forms of energy. Here we will discuss about pyranine, a photoacid.

Irreversible photoacids, commonly referred to as photoacid generators (PAGs), undergo a photochemical transformation that results in the formation of very strong acids, leading to a high concentration of protons. While some PAGs may exhibit reversible pathways in their mechanisms,[13] they are predominantly characterized by their irreversible nature. In contrast, reversible photoacids are advantageous because they allow not only the initiation of a process through light exposure but also the ability to stop or reverse that process by turning off the light, thus providing complete control over the reaction.

In the literature, the term "photoacid" typically refers to excited-state photoacids, which are molecules that exhibit high acidity in their excited states, such as naphthol derivatives. These compounds are reversible; when they relax from the excited state and back to the ground state, they revert to a lower acidity. These excited-state photoacids have been studied since the 1970s.[14-17] However, achieving a significant increase in proton concentration with excited-state photoacids is challenging due to their rapid relaxation from the high-acidity excited state to the low-acidity ground state. This limitation has led to interest in metastable photoacids (mPAHs), which can maintain a higher proton concentration for longer durations, providing a more effective means of controlling proton transfer processes.

Recently developed metastable-state photoacids are capable of generating a significant concentration of protons with high efficiency and good reversibility.[18] These metastable-state photoacids are typically designed by connecting an electron-accepting **(EA)** moiety to

a weakly acidic nucleophilic moiety **(NuH)** via a double bond **(Figure 1.3)**, allowing them to absorb and be activated by visible light. Upon light exposure, the photoinduced trans-cis isomerization of the double bond facilitates a nucleophilic reaction between the two moieties, resulting in the formation of a highly acidic metastable state that releases a proton. Under dark conditions, this metastable state can revert to its original form, reclaiming the proton. The reverse reaction is also multistep, with the half-life of the acidic state often depending on concentration; at concentrations between 10^{-5} and 10^{-3} M, different metastable-state photoacids exhibit half-lives ranging from seconds to hours. Due to their extended lifetime, the photogenerated acidic form can accumulate to high concentrations even under moderate light intensity, typically from visible light LEDs or sunlight.

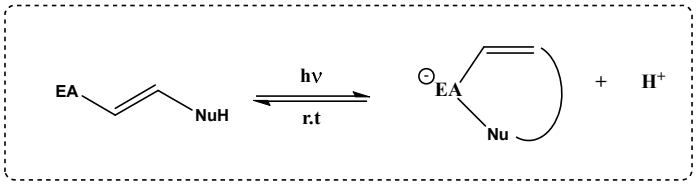

Figure 1.3. Designing of meta stable

Pyranine **(Figure 1.4A)** is an aryl sulfonate compound that contains a hydroxyl group and can exist in either a protonated form (ROH) or a deprotonated form (RO^-), with their excited states denoted as ROH^* and RO^{-*}. The photophysical characteristics of pyranine have been explored for decades by researchers such as Ireland, Wyatt[19] and Förster[20], who investigated the acidity in an excited state of various aryl compounds. The Förster cycle elucidates the energy transitions between ROH and RO^- **(Figure 1.4B),** signifying the acid-base equilibrium and showing their specific properties in both ground and excited states. The transition energy required for the (S_0)-ground state to the (S_1)-first excited state transition differs between ROH and RO^-, leading to variations in wavelengths of absorption and emission for the two states of pyranine. For pyranine, the absorption peaks for the ROH state are approximately 400 nm, while its emission occurs around 445 nm. In contrast, the RO^- state has absorption at about 460 nm and emission at approximately 510 nm. Additionally, the different Gibbs free energy

change (ΔG) associated with the acid-base transition [ROH ↔ RO^- + H^+] in between the ground (ΔG) and excited states (ΔG^*), where ΔG is greater than ΔG^*. This results in a significant difference in values of pK_a: pK_a of the ground state is around 7.3–7.7, while the pK_a^* of the excited state ranges from 0.4 to 1.3.

In the case of pyranine as a photoacid, the acid-base transition can be analyzed similarly to any Bronsted–Lowry acid, requiring a proton acceptor, typically water in addition to photoacid, i.e. pyranine as the proton donor. The photoprotolytic cycle involving pyranine and water **(Figure 1.4C)** emphasizes its various applications as a fluorescent probe. While numerous photoacids exhibit significant ΔpK_a values and similar excited-state proton transfer processes, such as photoacids based on naphthol and photoacids based on hydroxycoumarin.[21-23] However pyranine remains the most widely utilized fluorescent probe in this category due to several advantages: its absorption and emission bands fall within the visible spectrum, it's high solubility in water and is charged negatively across a broad range of pH due to its sulfonate groups, and its pK_a value is close to physiological pH.

Here we have recorded the excitation and emission spectra of pyranine (1 μM) in an aqueous solution of [Phosphate-Citrate buffer for pH 4], in [Sodium Phosphate buffer for pH 7], in [Carbonate-Bicarbonate buffer for pH 10], recorded in a fluorometer **(Figure 1.4D).** In this study, we also investigated the pH titration of 200 μM-pyranine in the presence of blue light. Initially, the pH of the pyranine solution was maintained at about 6.6, After exposing the solution to blue light (440 nm) for a few hours, the pH drop was observed consistent to 3.9-4.0, indicating a shift to an acidic range **(Figure 1.4E).** When we returned the exposed pyranine solution to darkness, no reversibility in pH was observed, even after prolonged exposure to the dark. This indicates the irreversible behaviour of pyranine.

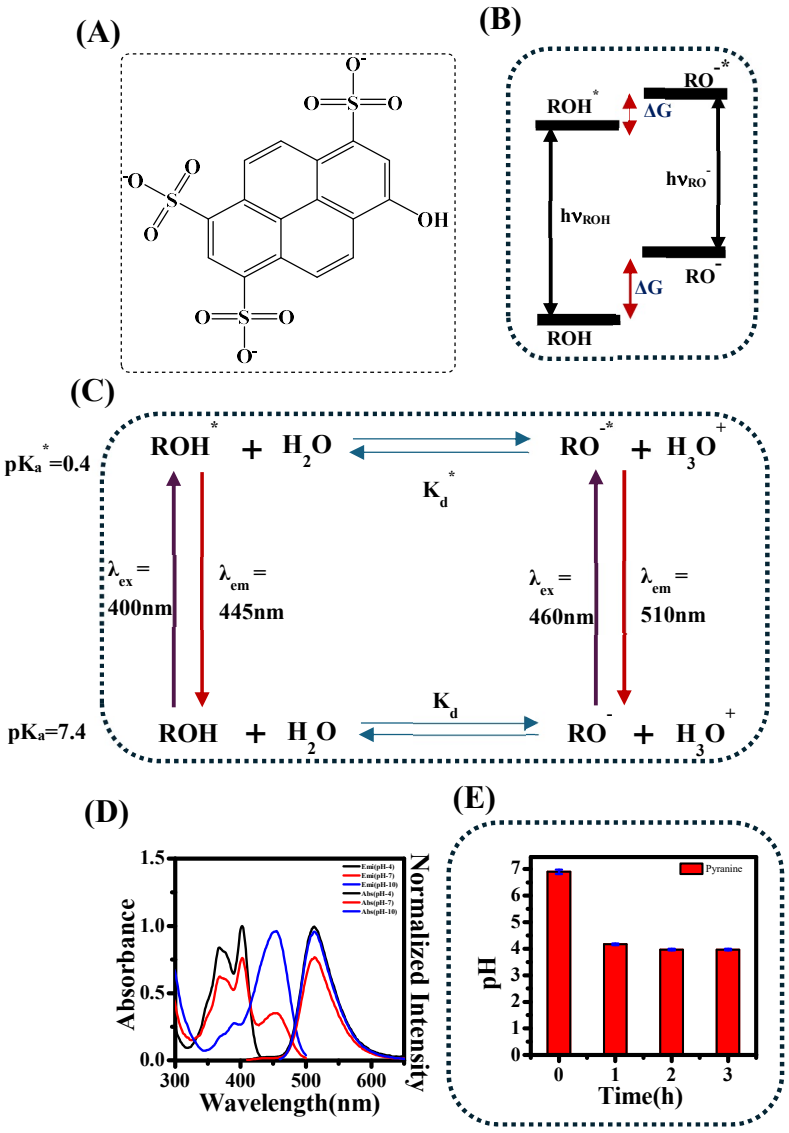

Figure 1.4. (A) Pyranine fluorescent probe, **(B)** Förster cycle, **(C)** Photoprotolytic cycle, **(D)** Emission (λ_{ex} **= 400 nm)** and Excitation (λ_{em} **= 510 nm)** spectra of pyranine in aqueous buffer solutions at pH 4 **(black)**, pH 7 (red), and pH 10 (blue), **(E)** pH titration of 200 μM-Pyranine in blue light.

1.9 Photobases:

Molecules that demonstrate enhanced basicity when exposed to light are known as Photobases. This photobasic property empowers them to efficiently withdraw protons from their surroundings, enabling them to regulate proton transfer processes in a light-controlled fashion. Photobases are characterized by a greater affinity for protons in their excited states relative to their ground states, which allows them to readily accept protons from nearby molecules, including water, upon light activation.

1.10 Doxorubicin (DOX):

DOX, also known by its trade name Adriamycin, is a widely used chemotherapeutic agent that belongs to the anthracycline class of antibiotics. Originally isolated from the bacterium Streptomyces paucities in the 1960s, doxorubicin has become a cornerstone in the treatment of a broad range of cancers, including breast, lung, ovarian, bladder, thyroid, soft tissue sarcomas, lymphomas, and leukaemias.[24-25] Its clinical success is attributed to its potent cytotoxic activity against rapidly dividing cells and its ability to target multiple intracellular pathways.

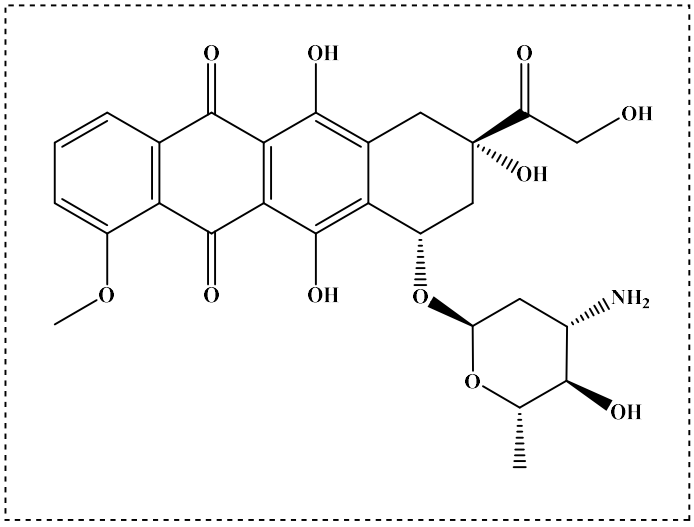

Figure 1.5. Structure of DOX

CHAPTER 2: PAST WORK

2.1 Review of Past Work and Project Motivation:

Recent research has highly focused on developing nanocomposites that are self-assembled and multifunctional, such as colloidal coacervate droplets, hydrogels, and hybrid vesicles, due to their significant potential in fundamental scientific studies.[26-30] Although there is high complexity in fabricating and designing these nanocomposites, and also being time-consuming, the spontaneous self-assembly of mixtures containing polyelectrolytes that are oppositely charged, into spherical coacervate droplets offers a simpler alternative. Coacervation is a spontaneous process of liquid-liquid phase separation that occurs in aqueous solutions containing oppositely charged polyelectrolytes. This phenomenon leads to the formation of spherical, self-assembled coacervate droplets that exhibit liquid-like properties due to electrostatic interactions. Coacervates are especially important in the study of artificial protocells due to their membrane-less structure, which allows them to selectively sequester a wide range of enzymes, organic molecules and proteins.[31-33] Research has demonstrated that the spontaneous sequestration process is affected by both hydrophobic and electrostatic interactions between the guest molecules and the coacervate droplets.

Earlier studies on coacervate droplets lacked intrinsic fluorescence, limiting their utility in optical applications. In a pioneering advancement, Vaishnav *et al.* engineered luminescent hybrid coacervate droplets through the electrostatic interaction of CdTe QDs and PDADMAC in aqueous media. These droplets demonstrated exceptional stability across a broad range of pH, ionic strengths, and compositions. Characterization via confocal CLSM and epifluorescence imaging revealed their inherent bright photoluminescence, high photostability, and resistance to photo bleaching. The coacervation mechanism is driven by electrostatic attraction between negatively charged CdTe QDs and cationic PDADMAC chains. Furthermore, these hybrid droplets exhibited

selective uptake of organic dyes and serum albumin proteins, underscoring their potential as versatile carriers for bioimaging and therapeutic delivery.

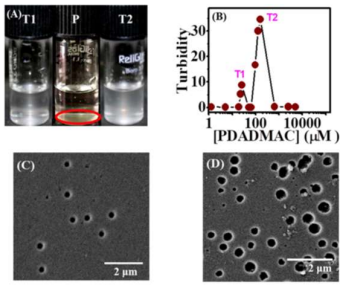

Figure 1.6. (A) T1, P and T2 region of QD-PDADMAC binary solution. **(B)** Plot of turbidity v/s concentration of PDADMAC. FESEM images of the droplets at the **(C)** T1 and **(D)** T2 region.

The stability of the coacervate droplets under varying pH and ionic strength conditions was systematically analyzed. Turbidity measurements indicated that mixtures in the T1 and T2 regions remained opaque between pH 6.0 and 10.0, transitioning to a uniform state at more acidic levels (pH 3.0–5.5). A sigmoidal relationship between turbidity and pH revealed a critical coacervation threshold at pH 6.0. FESEM imaging at pH 3.0 confirmed structural disassembly **(Figure 1.7A, inset)**, while stability persisted until pH 11.7. Protonation of MSA ligand carboxylate groups ($pK_a \approx 4.19$ and 5.64) on the QD surface at lower pH weakened electrostatic interactions with PDADMAC, driving disassembly. This pH-dependent behavior highlights their suitability for biomedical applications requiring controlled release. Similarly, increasing ionic strength reduced turbidity, with a critical NaCl concentration of 120 mM identified, beyond which electrostatic interactions between QDs and PDADMAC were effectively screened **(Figure 1.7B).**

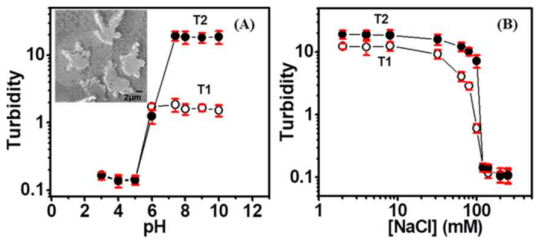

Figure 1.7. (A) Changes in the turbidity of the QD-PDADMAC mixture as a function of solution pH in the T1 and T2 regions. The inset shows the FESEM image of the T1 region at pH 3. **(B)** Changes in the turbidity of the QD-PDADMAC mixture as a function of NaCl concentration in the T1 and T2 regions.

The earlier mentioned coacervate systems utilizing QDs, faced limitations due to their inherent toxicity and lack of biocompatibility. Addressing this, Saini *et al.* engineered CD-based coacervate NDs via electrostatic coacervation of anionic CDs with the cationic polymer PDADMAC. These NDs were comprehensively characterized using advanced spectroscopic and microscopic techniques, revealing their intrinsic porous nanostructure capable of sequestering dyes and therapeutic agents without structural modification. Notably, the cationic anticancer drug (DOX) exhibited a high partition coefficient (10.6 ± 1.1) within the NDs, underscoring their drug-loading efficiency.

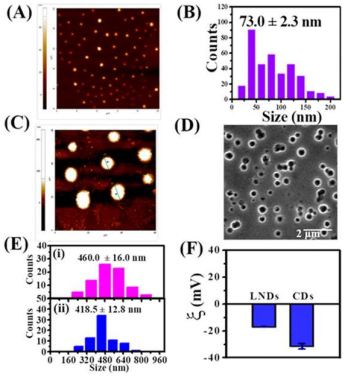

Figure 1.8. **(A)** AFM image of SNDs **(B)** Size distribution histogram **(C)** AFM image of LNDs **(D)** FESEM image of LNDs. **(E)** Size distribution histogram with their mean sizes estimated from (i) FESEM and (ii) AFM height profile. **(F)** Estimated ζ-potentials of CDs and LNDs.

The stability of self-assembled NDs under varying pH and ionic strength was systematically investigated. Turbidity analysis of the CD-PDADMAC binary mixture revealed a pH-dependent phase transition: the system remained turbid within pH 5.5-12 but transitioned to a transparent state below pH 5.5, with complete disassembly observed at pH 4.8-2.0 **(Figure 1.9A).** This disassembly correlates with protonation of carboxylate groups on the CD surface, weakening electrostatic interactions with cationic PDADMAC. Similarly, increasing ionic strength (via NaCl addition) reduced turbidity, with full dissolution occurring at ≥400 mM NaCl **(Figure 1.9B)**, indicative of electrostatic screening between CDs and PDADMAC. These results underscore the NDs' stability across broad pH and ionic conditions, governed by electrostatic-driven assembly. Such robustness highlights their potential for applications requiring controlled structural integrity in dynamic environments.

Inspired by these findings, this work aims to engineer optically active coacervate droplets capable of light-triggered assembly and disassembly under physiological conditions. By leveraging light as a non-invasive stimulus, we seek to achieve spatiotemporal control over the selective sequestration of photoactive molecules (e.g., pyranine) and therapeutic agents (e.g., DOX). This approach enables precise, on-demand drug release, addressing critical challenges in targeted therapies such as minimizing off-target effects in cancer treatment while advancing the development of adaptive biomaterials for biomedical applications.

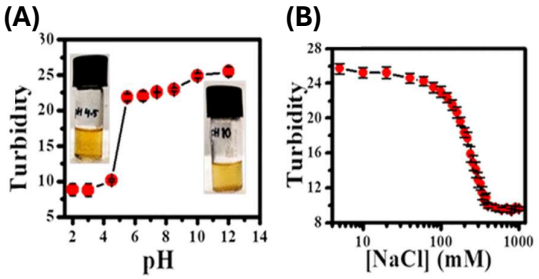

Figure 1.9. Changes in the turbidity of ND dispersion as a function of **(A)** pH and **(B)** NaCl concentrations.

CHAPTER 3: EXPERIMENTAL SECTION

3.1. Materials:

Cadmium chloride ($CdCl_2$), mercaptosuccinic acid (MSA), sodium tellurite (Na_2TeO_3), trisodium citrate dehydrate, Citric acid monohydrate (99.5%) was purchased from Merck (Germany), Ethylenediamine (EDA, 99.5%), poly(diallyldimethylammonium chloride) (PDADMAC, MW =100000-200000), Sodium borohydride ($NaBH_4$) was procured from SRL, DI water, Adenosine 5'-triphosphate (ATP) from Sigma-Aldrich, sodium hydroxide (NaOH), hydrochloric acid (HCl), Doxorubicin hydrochloride (>95.0%) was procured from Sigma-Aldrich, 8-Hydroxypyrene-1,3,6-trisulphonicacid trisodium salt (>96.0%) was procured from TCI. Hellmanex III, and the Pur-A-Lyzert dialysis kit (molecular weight cutoff 3.5 kDa) were procured from Sigma-Aldrich.

3.2. Instrumentation:

Absorption spectra measurements were conducted with a Varian UV-vis spectrophotometer (Cary 100 Bio) using a (1 × 1 cm) quartz cuvette. Fluorescence spectra were acquired on a Fluoromax-4 spectrofluorometer (HORIBA Jobin Yvon, FM-100) with excitation and emission slit widths fixed at 2 nm. Fourier-transform infrared (FTIR) spectroscopy was performed on a Bruker Tensor-27 spectrometer, with samples prepared as KBr pellets. Zeta potential and particle size measurements utilized a NanoBrook analyser. Confocal laser scanning microscopy (CLSM) images were captured using an Olympus FV1200MPE inverted microscope equipped with a 100x oil immersion objective (NA 1.4). Excitation wavelengths of 405, 488, and 559 nm were applied with corresponding dichroic mirrors and emission filters (blue channel: 410–490 nm; green channel: 490–565 nm; red channel: 575–675 nm). For CLSM, samples were drop-cast onto cleaned glass slides and desiccated overnight.

3.3. Synthesis of ATP Droplets:

To synthesize ATP droplets, we first prepare a stock solution of ATP at a concentration of 0.6 M. This is done by adding 82.65 mg of ATP to 250 µL of deionized (DI) water at pH 7.4 and sonicating the mixture. Next, take an Eppendorf tube and add 3 mL of DI water to it. Then add 1.002 mM ATP and 1.28 M of the polymer (PDADMAC) to the Eppendorf tube. Allow the mixture to equilibrate for 1 h, during which ATP droplets will form **(Scheme 3)**.

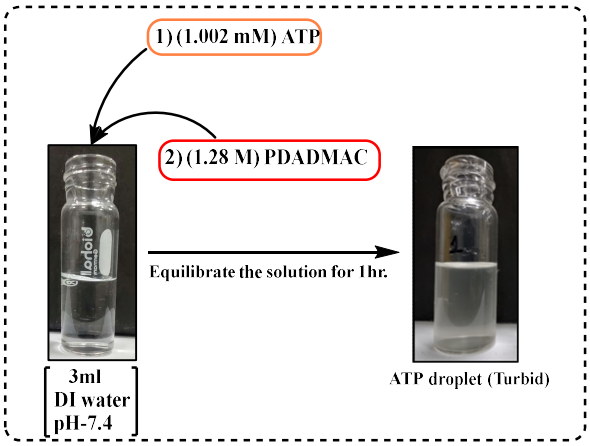

Scheme 3. Synthesis scheme of ATP droplets.

3.4 Sequestration of pyranine in ATP droplets:

The equilibrium partition coefficients (K) of pyranine in ATP-containing coacervate droplets were determined via UV-visible spectroscopy. ATP coacervates were isolated by centrifugation (16000 rpm, 30 min), redispersed in aqueous medium, and mixed with 20 µM pyranine solutions, then equilibrate for 15 minutes. After equilibration, the mixtures were centrifuged again (16000 rpm, 30 min) to separate the coacervate-rich phase from the supernatant. Pyranine concentrations in the supernatant were quantified using UV-visible absorbance measurements. The partition coefficient was calculated as the ratio of pyranine concentration in the coacervate phase to that remaining in the supernatant.

3.5 Photo-responsive nature of ATP droplets in the presence of photoacid (pyranine):

In this experiment, we investigated the sequestration of pyranine in ATP droplets and monitored the behaviour of these droplets in the presence of blue light (440 nm) **(Figure 1)**. To begin, take a cuvette and add the (3 mL) ATP droplets to it, followed by the addition of 100 µM pyranine solution. Record the UV spectrum of this solution. Next, expose the solution to blue light (440 nm) for 1 h and immediately record the UV spectrum. Afterwards, drop cast the solution onto clean glass slides for (CLSM) analysis.

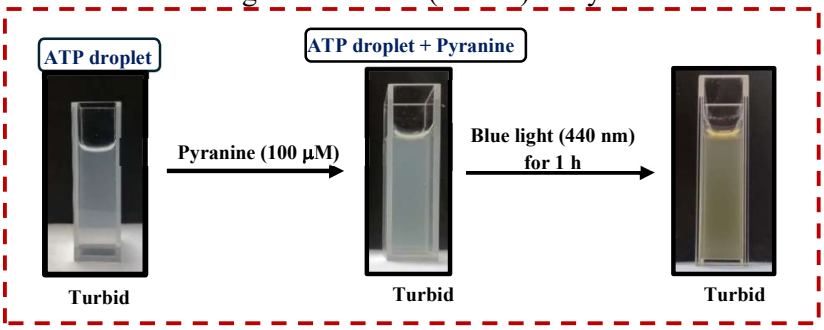

Figure 1. Pathway for photo-responsive nature of ATP droplets in the presence of pyranine.

3.6 Synthesis of MSA-capped CdTe red QDs.

To synthesize the MSA-CdTe red quantum dots, 4 mL of a 0.04 M $CdCl_2$ solution was first diluted to a total volume of 50 mL in a 100 ml round bottom flask. Then, trisodium citrate dihydrate (100 mg), MSA (50 mg), 1 mL of a 0.01 M Na_2TeO_3 solution, and $NaBH_4$ (100 mg) were added while continuously stirring the mixture. The stirring continued until the colour of the solution changed to green.

Next, attached the round bottom flask to a condenser and refluxed it for 18 h, under open-air conditions in a 100˚C silicon oil bath, to produce red-emitting QDs. Afterwards, the dialysis of the resulting CdTe QD solution was performed using a dialysis membrane (Molecular weight cutoff 3.5 kDa) against DI-water for 24 h. The purified quantum dots were synthesized **(Scheme 4).** Stored it at 4˚C for future use.

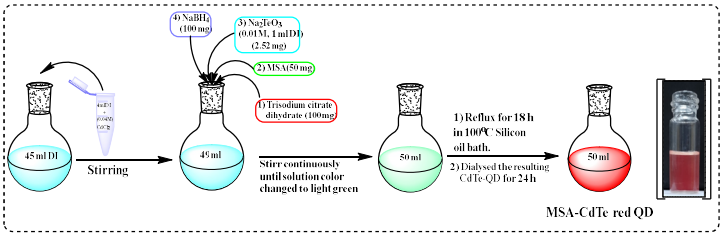

Scheme 4. Synthesis scheme of MSA-CdTe red QDs.

3.7 Synthesis of MSA-capped CdTe red QD droplets.

To synthesize QD droplets, begin by adding 3 mL of DI water (pH=7.0) to a glass vial, then add 175 µL of MSA-capped red QDs and 76 µM of PDADMAC polymer. Allow the solution to equilibrate for 4 h, during which the droplets will form **(Scheme 5).**

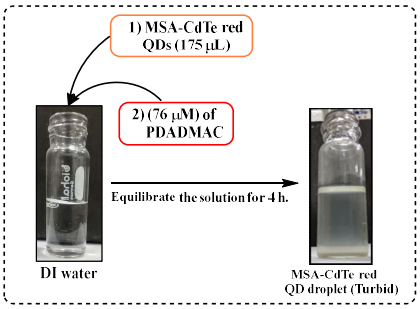

Scheme 5. Synthesis scheme of MSA-CdTe red QD droplets.

3.8 Sequestration of solutes in MSA-CdTe red QD droplets:

The equilibrium partition coefficients (K) of different solutes in MSA-capped CdTe QD droplets were determined via UV-Visible spectroscopy. QD coacervates were isolated by centrifugation (16,000 rpm, 30 min), redispersed in aqueous medium, and mixed with pyranine (19.5 µM) and DOX (19.5 µM) solutions, then equilibrate for 1 h . After equilibration, the mixtures were centrifuged again (10,000 rpm, 30 minutes) to separate the coacervate-rich phase from the supernatant. Solutes concentration in the supernatant was quantified using UV-Visible absorbance measurements. The partition coefficient was calculated as the ratio of solute concentration in the coacervate phase to that remaining in the supernatant.

3.9 Photo-responsive nature of MSA-CdTe red QD droplets in the presence of photoacid (pyranine):

In this experiment, we investigated the sequestration of pyranine in MSA-CdTe QD droplets and monitored the behaviour of these droplets in the presence of blue light (440 nm) at different time intervals **(Figure 2).** To begin, take a glass vial and add the (3 mL) MSA-CdTe red QD droplets to it, followed by the addition of 200 µM pyranine solution & then incubate it for 15 minutes. Next, expose the solution to blue light (440 nm) for 1, 2 & 3 h along with their control samples. Afterwards, drop cast them onto clean glass slides for (CLSM) analysis.

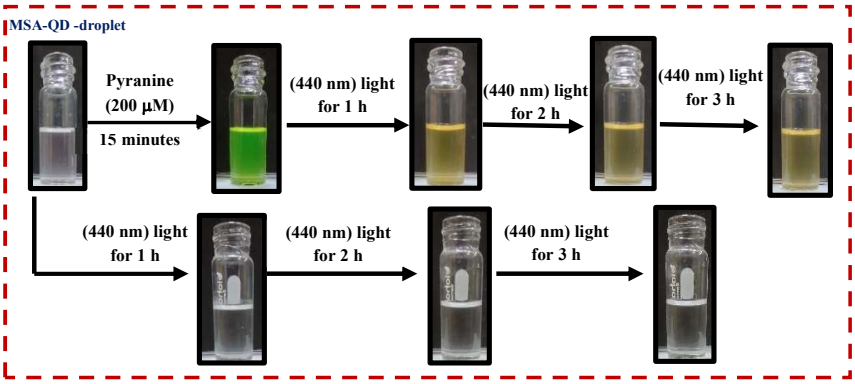

Figure 2. Pathway for photo-responsive nature of MSA-CdTe red QD droplets in the presence of pyranine.

3.10 Synthesis of CDs.

The synthesis of colloidal carbon dots (CDs) was accomplished using a hydrothermal approach. The process began by dissolving 1.015 g of citric acid in 10 mL of DI water, followed by 5 minutes of sonication. Following complete dissolution, 335 µL of ethylenediamine was introduced, and the mixture underwent an additional 5 minutes of sonication. The resulting solution was then transferred to a Teflon-padded autoclave with a 25 mL capacity. This vessel was sealed and subjected to heating at 200˚C for a duration of 5 h. After the reaction period, the autoclave was allowed to cool naturally to r.t. To purify the synthesized CDs, the reaction product underwent dialysis using a specialized dialysis kit Pur-A-Lyzert (Molecular weight cutoff 3.5 kDa)

(**Scheme 6)**. This step served to eliminate any residual unreacted precursors from the final CD suspension.

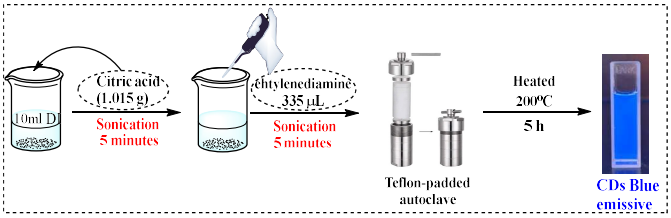

Scheme 6. Synthesis scheme of CDs.

3.11 Synthesis of CD droplets.

The fabrication of carbon dot nanodroplets (NDs) was achieved by combining carbon dots (CDs) and PDADMAC in an aqueous solution. The process involved mixing of 50 µL CDs with 32 µM PDADMAC **(Scheme 7)**. The pH of the mixture was adjusted to 10 using 0.1 M sodium hydroxide. This preparation was then allowed to equilibrate at room temperature for 2 h, resulting in the formation of the desired NDs.

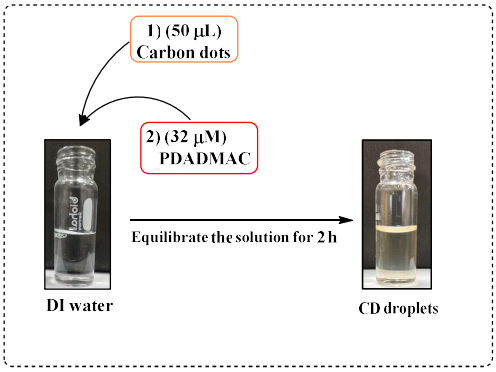

Scheme 7. Synthesis scheme of CD droplets

3.12 Sequestration of solutes in CD droplets:

The equilibrium partition coefficients (*K*) of different solutes in CD droplets were determined via UV-Visible spectroscopy. CD coacervates were isolated by centrifugation (16,000 rpm, 30 min), redispersed in aqueous medium, and mixed with pyranine (20 µM) and DOX (20 µM) solutions, then equilibrated for 15 minutes and 24 h,

respectively. After equilibration, the mixtures were centrifuged again (10,000 rpm, 30 min) to separate the coacervate-rich phase from the supernatant. solutes concentrations in the supernatant were quantified using UV-Visible absorbance measurements. The partition coefficient was calculated as the ratio of solute concentration in the coacervate phase to that remaining in the supernatant.

3.13 Photo-responsive nature of CD droplets in the presence of photoacid (pyranine):

In this experiment, we investigated the sequestration of pyranine in CD droplets and monitored the behaviour of these droplets in the presence of blue light (440 nm) at different time intervals **(Figure 3).** To begin, take a glass vial and add the 3 ml CD droplets to it, followed by the addition of 30 µM pyranine solution & then incubate it for 15 minutes. Next, expose the solution to blue light (440 nm) for 1, 2 & 3 h along with their control samples. Afterwards, drop cast them onto clean glass slides for (CLSM) analysis.

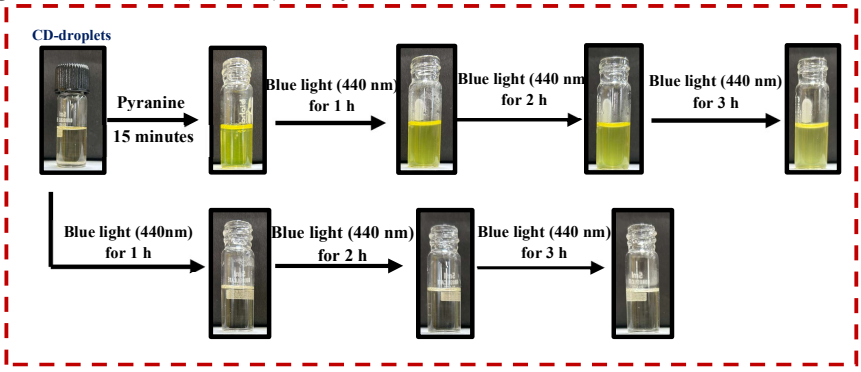

Figure 3. Pathway for the photo-responsive nature of CD droplets in the presence of pyranine.

CHAPTER 4: RESULTS AND DISCUSSION

4.1 Characterization of ATP droplets:

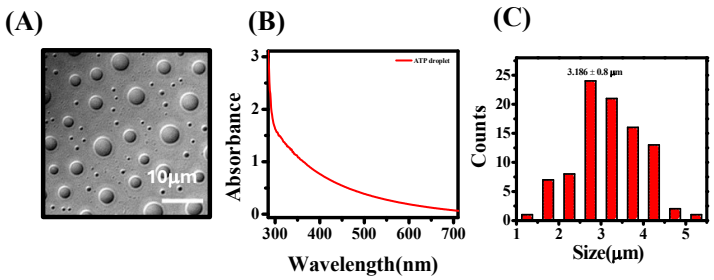

Figure 4. (A) CLSM, **(B)** UV-visible, and **(C)** Size distribution histogram of ATP droplets.

The ATP coacervate droplets, synthesized through electrostatic interaction with cationic polymers, were characterized using complementary analytical techniques (CLSM). (CLSM) Imaging **(Figure 4A)** revealed the spherical morphology and uniform distribution of the ATP droplets, confirming successful coacervation. Concurrent UV-visible spectroscopic analysis **(Figure 4B)** demonstrated characteristic absorption bands that further validated the formation of ATP coacervate droplets. To assess size uniformity and dispersion characteristics, a detailed size distribution histogram was conducted; the resulting histogram **(Figure 4C)** exhibited a relatively narrow size distribution with a mean diameter of (3.186 ± 0.8 µm), indicating the formation of microscale coacervate droplets with good monodispersity. This microscale dimension is particularly advantageous for potential biomedical applications, as it facilitates cellular uptake and enhances bioavailability.

Characterization of Pyranine Sequestration in ATP droplets:

To examine the sequestration capabilities of ATP droplets, we conducted experiments using pyranine. We utilized UV-visible spectroscopy to analyze the sequestration behaviour of pyranine within

the ATP droplets by calculating the equilibrium partition coefficient (K) **(Table 1)**. High value of K for pyranine represents its good sequestration in ATP droplets. This approach allowed us to evaluate how effectively the droplets could capture and retain this molecule, providing insights into their potential applications in observing photo-responsive assembly and disassembly.

Solutes	Concentration (μM)	*K*
Pyranine	20	7.58 ± 1.2

Table 1. Equilibrium partition coefficient of pyranine in ATP droplets.

Investigation of Light-Responsive Behaviour:

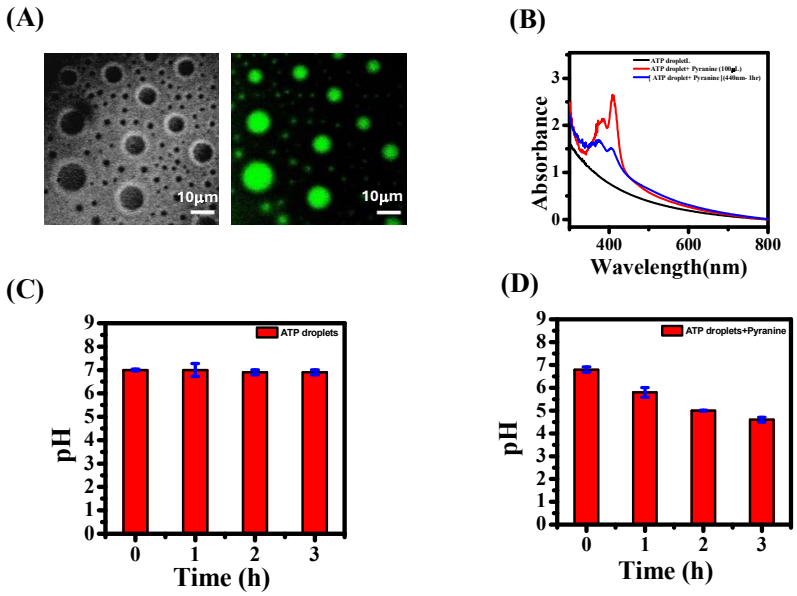

Figure 5. **(A)** CLSM image of pyranine-loaded ATP droplets in the presence of blue light (440 nm) for 1 h, and **(B)** their UV-visible spectra. **(C)** pH titration of ATP-droplets in blue light, and **(D)** Pyranine loaded ATP-droplets in blue light.

We investigated the potential light-responsive behaviour of ATP droplets by incorporating pyranine, a well-documented photoacid

capable of releasing protons upon light exposure. To evaluate photoacid-induced structural changes, pyranine-loaded ATP droplets were exposed to continuous illumination with blue light (440 nm) for 1 h. CLSM imaging revealed no significant disassembly of the droplet structure during this period **(Figure 5A)**. The corresponding UV-visible spectroscopic analysis **(Figure 5B)** revealed the characteristic absorption bands of both ATP and pyranine, confirming the presence of both components within the system.

pH-Dependent Stability Analysis:

To elucidate the factors influencing droplet stability under light stimulation, systematic pH titration experiments were conducted. Firstly, we did the pH titration of ATP droplets in presence of blue light (440 nm) **(Figure 5C)**. Subsequently, pH titrations were performed on pyranine-loaded ATP droplets subjected to blue light (440 nm) illumination for progressively increasing durations (1, 2, and 3 h) **(Figure 5D)**. These time-dependent pH titration experiments provided crucial insights into the relationship between light exposure, proton generation, and droplet stability. The results indicated that while pyranine undergoes photoactivation upon blue light illumination, the local pH changes generated within the ATP droplet environment were insufficient to trigger complete disassembly within the timeframe studied. This observation suggests that ATP coacervate droplets possess remarkable buffer capacity or structural resilience against photoacid-induced pH changes.

4.2 Characterization of MSA-capped CdTe red QD:

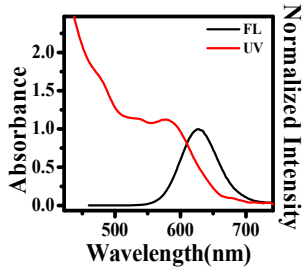

Figure 6. UV-visible and Fluorescence spectra of MSA-CdTe red QD.

The as-synthesized MSA-capped CdTe red Quantum dot are characterized using UV-visible and Fluorescence spectra **(Figure 6).** The exciton band maximum appears at 578 nm. A sharp PL peak appears at 627 nm.

4.3 Characterization of MSA-capped CdTe red QD droplets:

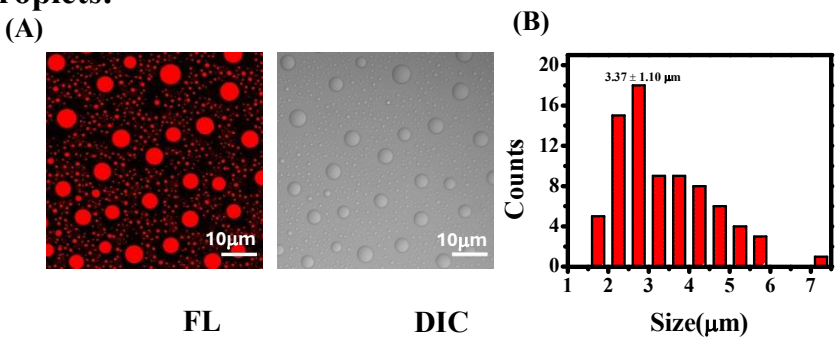

Figure 7. (A) CLSM & **(B)** Size distribution histogram of MSA-CdTe red QD droplets.

The QD coacervate droplets, were characterized using complementary analytical techniques (CLSM). (CLSM) Imaging **(Figure 7A)** revealed the spherical morphology and uniform distribution of the QD droplets, confirming successful coacervation. To assess size uniformity and dispersion characteristics, a detailed size distribution histogram was conducted; the resulting histogram **(Figure 7B)** exhibited a relatively narrow size distribution with a mean diameter of (3.37 ± 1.10 μm).

Characterization of Solutes Sequestration in MSA-capped CdTe red QD droplets:

To examine the sequestration capabilities of MSA-capped CdTe red quantum dot droplets, we conducted experiments using two different solutes: pyranine and the anticancer drug doxorubicin (DOX). We utilized UV-visible spectroscopy to analyze the sequestration behaviour of these substances within the QD droplets by calculating the equilibrium partition coefficient (*K*) **(Table 2)**. High value of *K* for pyranine represents its good sequestration in QD droplets, while the

value of *K* for DOX is very less, representing its poor efficiency to get encapsulated in QD droplets. This approach allowed us to evaluate how effectively the droplets could capture and retain these molecules, providing insights into their potential applications in drug delivery and loading.

Solutes	Concentration (μM)	*K*
Pyranine	19.5	56.32 ± 5.6
DOX	19.5	1.33 ± 0.196

Table 2. Equilibrium partition coefficient (*K*) of pyranine and DOX in QD droplets.

Investigation of Light-Responsive Behaviour:

Our study explored the light-induced responsiveness of quantum dot (QD) droplets through the incorporation of pyranine, a recognized photoacid that generates protons when exposed to light. We subjected both pyranine-loaded QD droplets and unmodified control samples to systematic illumination with blue light (440 nm) for periods of 1, 2, and 3 h, to assess structural modifications triggered by photoacid activation. CLSM analysis revealed distinct behavioral differences between the two systems. The control QD droplets maintained their structural integrity throughout the illumination period for 0, 1, 2 & 3 h **(Figure 8. A, B, C & D, respectively)**, while the pyranine-containing QD droplets exhibited progressive disassembly under illumination period for 0, 1, 2 & 3 h **(Figure 9. A, B, C & D, respectively)**. This differential response demonstrates the critical role of pyranine in mediating light-triggered structural changes within the QD droplet architecture.

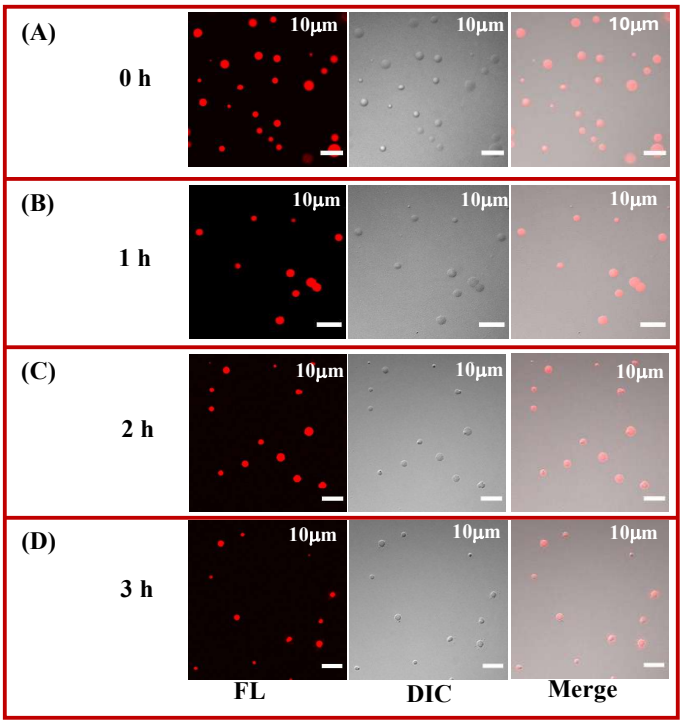

Figure 8. CLSM image of QD droplets control in the presence of blue light for **(A)** 0 h, **(B)** 1 h, **(C)** 2 h & **(D)** 3 h respectively.

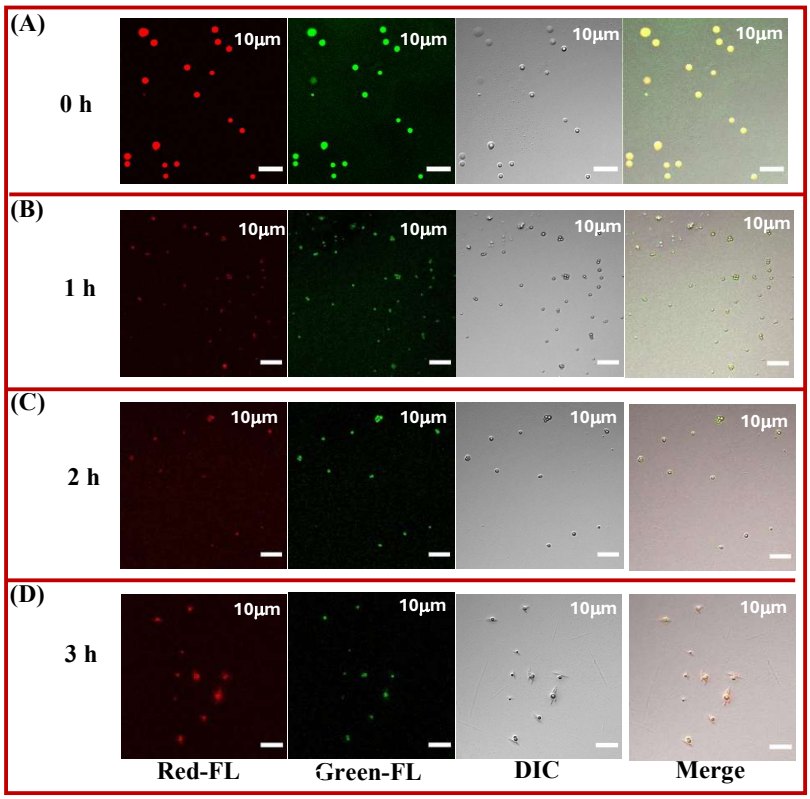

Figure 9. CLSM image of pyranine-loaded QD droplets in the presence of blue light for (A) 0 h, (B) 1 h, (C) 2 h & (D) 3 h, respectively.

pH-Dependent Stability Analysis:

To elucidate the factors influencing pyranine-loaded droplets disassembly under light stimulation, systematic pH titration experiments were conducted. Firstly, we did the pH titration of QD droplets in the presence of blue light (440 nm) **(Figure 10A)**. Subsequently, pH titrations were performed on pyranine (200 μM)-loaded QD droplets subjected to blue light (440 nm) illumination for progressively increasing durations (1, 2, and 3 h) **(Figure 10B)**. These time-dependent pH titration experiments provided crucial insights into the relationship between light exposure, proton generation, and droplet stability. The results indicated that while pyranine undergoes photoactivation upon blue light illumination, the local pH changes generated within the QD droplet environment were sufficient to trigger complete disassembly within the timeframe studied.

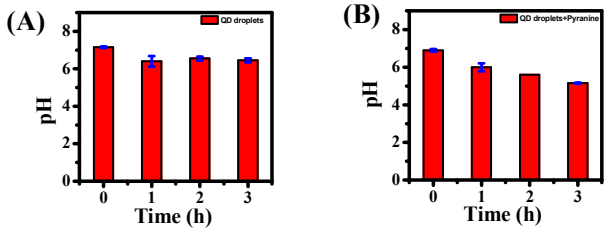

Figure 10. (A) pH titration of QD-droplets in blue light, and **(B)** pyranine-loaded QD-droplets in blue light.

4.4 Characterization of CDs:

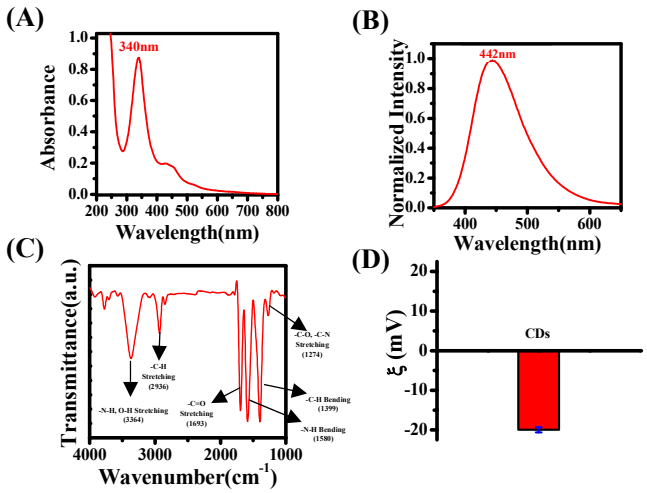

Figure 11. (A) UV-visible, **(B)** Fluorescence spectra, **(C)** FTIR spectra and **(D)** ζ-potential of CDs.

The as-synthesized CDs underwent comprehensive analysis using multiple spectroscopic techniques to determine their optical and surface properties. Analysis of the UV-visible absorption spectrum **(Figure 11A)** revealed a primary peak at 340 nm, attributed to n-π* electronic transitions occurring at carbonyl groups on the CD surface. Additionally, a weak shoulder near 250 nm was observed, corresponding to π-π* transitions within the aromatic carbon sp^2 framework of the CD core. Fluorescence characterization conducted at an excitation wavelength of 340 nm **(Figure 11B)** demonstrated that these CDs emit strongly at 442 nm, producing a well-defined emission band. To identify the chemical functionality on the CD surface, FTIR spectroscopy was employed, as illustrated in **(Figure 11C).** The spectral data showed several characteristic bands: a broad signal around 3437 cm^{-1} corresponding to O-H and N-H stretching modes; C-H vibrations at 2967 cm^{-1} (stretching) and 1368 cm^{-1} (bending); carbonyl and amine signatures at 1690 cm^{-1} (C=O stretching) and 1569 cm^{-1} (N-H bending); and a band at 1274 cm^{-1} indicating C-O and C-N stretching modes. This FTIR profile confirms the presence of hydroxyl, amino, and carboxylic acid functional groups decorating the CD surface. Surface charge analysis through zeta potential measurements under basic conditions (pH 10) yielded a value of −19.97 ± 0.65 mV **(Figure 11D)**, indicating substantial negative surface charge resulting from the deprotonation of surface hydroxyl and carboxyl groups in alkaline medium.

4.5 Characterization of Carbon Dot droplets:

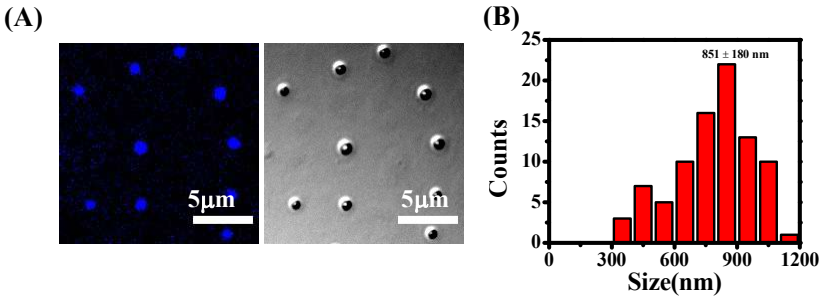

Figure 12. (A) CLSM & **(B)** Size distribution histogram of CD droplets.

The CD coacervate droplets, were characterized using complementary analytical techniques (CLSM). (CLSM) Imaging **(Figure 12A)** revealed the spherical morphology and uniform distribution of the CD droplets, confirming successful coacervation. To assess size uniformity and dispersion characteristics, a detailed size distribution histogram was conducted; the resulting histogram **(Figure 12B)** exhibited a relatively narrow size distribution with a mean diameter of (851 ± 180 nm), indicating the formation of nanoscale coacervate droplets with good monodispersity.

Characterization of Zeta Potential and Molecular Sequestration in Carbon Dot Droplets.

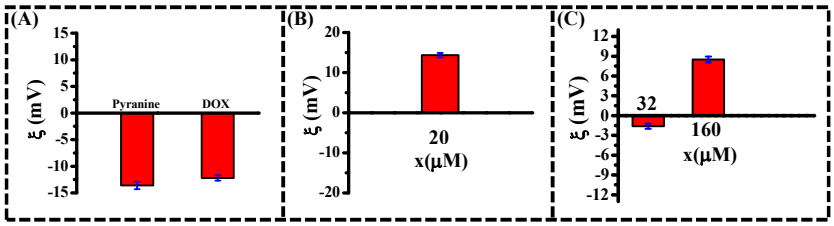

Figure 13. ζ-Potential of **(A)** Pyranine & DOX, **(B)** CD droplets at x=32 μM & 160 μM concentration of PDADMAC and **(C)** 20 μM pyranine loaded CD droplets.

To investigate the sequestration mechanisms of pyranine and DOX within CD droplets, we first determined the surface charge characteristics of each component through zeta potential measurements. Analysis revealed distinct electrokinetic profiles: pyranine exhibited a negative zeta potential of -13.6 ± 0.71 mV, while DOX showed a similar negative charge of -12.19 ± 0.5 mV at pH 10 **(Figure 13A).** The CD droplets, however, displayed concentration-dependent surface charge properties - at 32 μM of PDADMAC, the zeta potential measured -1.6 ± 0.39 mV, whereas at 160 μM PDADMAC, it shifted to a positive value of 8.51 ± 0.45 mV **(Figure 13B),** by keeping the concentration of CD fixed.

These opposing charge characteristics facilitated the examination of molecular sequestration dynamics. The negatively

charged pyranine molecules demonstrated preferential incorporation into positively charged CD droplets through complementary Electrostatic attractions and Hydrophobic interactions. We quantified this sequestration efficiency using UV-visible spectroscopy to determine the equilibrium partition coefficient (*K*) values **(Table 3).** The substantial *K* value obtained for pyranine indicated efficient sequestration within the CD droplets, which was further supported by the modified zeta potential 14.36 ± 0.56 mV of pyranine-loaded CD droplets **(Figure 13C).**

Subsequently, we examined the sequestration behaviour of equally concentrated, negatively charged DOX molecules in these pyranine-loaded CD droplets. The corresponding *K* values calculated from spectroscopic data confirmed effective DOX incorporation into the pyranine-loaded CD droplet system **(Table 3)**. This sequential loading strategy provided valuable insights into the capture and retention mechanisms of these molecular systems, highlighting their potential applications in controlled drug loading, targeted delivery, and stimuli-responsive release in therapeutic contexts.

	Solutes	Concentration (μM)	*K*
(A)	Pyranine	20	14.8 ± 2.1
(B)	DOX	20	2.56 ± 0.3

Table 3. Equilibrium partition coefficient (*K*) of **(A)** pyranine in CD droplets and **(B)** DOX in pyranine-loaded CD

Investigation of Light-Responsive Behaviour:

Our investigation examined the light-dependent behaviour of CD droplets loaded with pyranine, a known photoacid that releases protons upon light exposure. We conducted a comparative analysis by exposing both pyranine-loaded CD droplets and unmodified control samples to controlled blue light illumination (440 nm) for progressive durations (0, 1, 2, and 3 h) to evaluate structural alterations induced by photoacid activation. CLSM imaging revealed unexpected behavioural

differences between these systems. The unmodified CD droplets demonstrated gradual disassembly with increasing illumination time **(Figure 14A, B, C & D, corresponding to 0, 1, 2 & 3 h, respectively)**. Conversely, pyranine-containing CD droplets exhibited enhanced assembly during identical illumination periods **(Figure 15A, B, C & D, corresponding to 0, 1, 2 & 3 h, respectively)**. This contrasting behaviour-disassembly in controls versus assembly in pyranine-loaded samples highlights pyranine's significant role in reversing the typical light-induced structural transformations within the CD droplet framework, suggesting potential applications in programmable materials with customizable light responses.

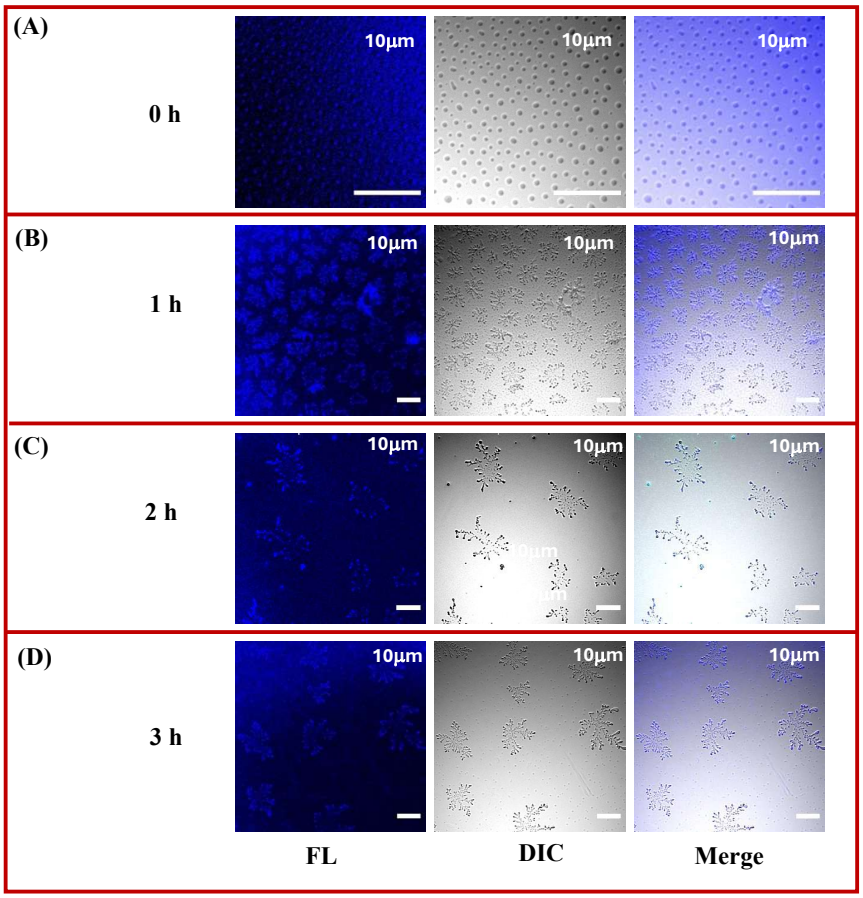

Figure 14. CLSM image of CD droplets control in the presence of blue light for **(A)** 0 h, **(B)** 1 h, **(C)** 2 h & **(D)** 3 h respectively.

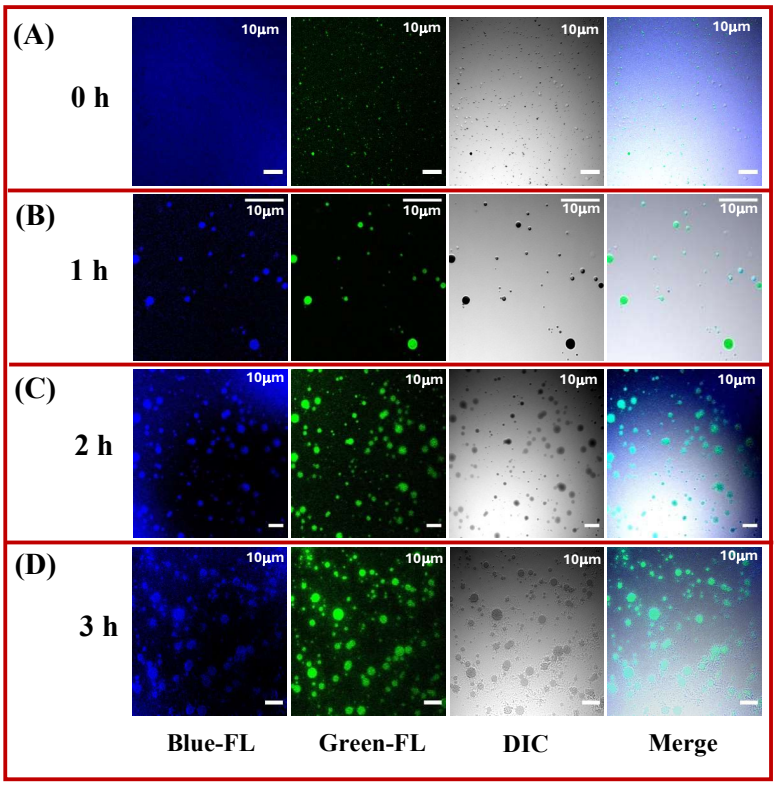

Figure 15. CLSM image of pyranine-loaded CD droplets in the presence of blue light for (A) 0 h, (B) 1 h, (C) 2 h, and (D) 3 h, respectively.

pH-Dependent Stability Analysis:

To elucidate the factors influencing pyranine-loaded droplets assembly under light stimulation, systematic pH titration experiments were conducted. Firstly, we did the pH titration of CD droplets in the presence of blue light (440 nm) **(Figure 16A)**. Subsequently, pH titrations were performed on pyranine (30 µM)-loaded CD droplets subjected to blue light (440 nm) illumination for progressively increasing durations (1, 2 and 3 h) **(Figure 16B)**. The results indicated that while pyranine undergoes photoactivation upon blue light illumination, the local pH changes generated within the CD droplet environment were insufficient to trigger complete disassembly within the timeframe studied. However, it could be possible that in the presence of light, these deprotonated negatively charged pyranine

interact electrostatically with the positively charged PDADMAC, which might lead to self-assembly and do the formation of droplets in the presence of light rather than the disassembly, suggesting light-triggered reorganization through polyelectrolyte complexation rather than pH-mediated disassembly.

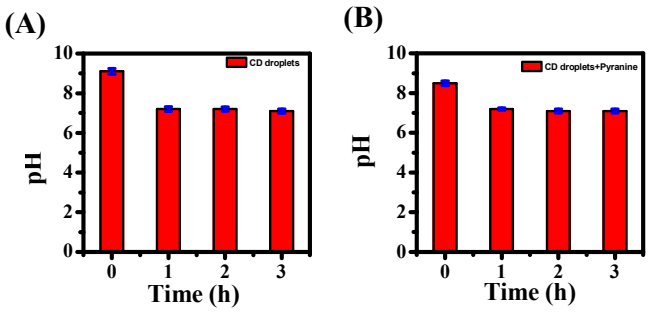

Figure 16. **(A)** pH titration of CD droplets in blue light, and **(B)** Pyranine loaded CD-droplets in blue light.

CHAPTER 5: CONCLUSION

This work presents a comprehensive investigation of three distinct coacervate systems: ATP droplets, MSA-capped CdTe red QD droplets, and CD droplets. Through systematic characterization and functional analysis, we have elucidated their unique sequestration properties and light-responsive behaviours, revealing promising applications in controlled drug delivery systems. The sequestration studies demonstrated that while pyranine was effectively incorporated across all three droplet systems, DOX exhibited selective sequestration only in pyranine-loaded CD droplets. Most significantly, our investigation revealed distinct photo-responsive profiles under blue light (440 nm) illumination. ATP droplets maintained structural integrity regardless of illumination duration. In contrast, pyranine-loaded QD droplets exhibited progressive disassembly upon prolonged exposure, indicating potential for light-triggered cargo release. Perhaps most interestingly, pyranine-loaded CD droplets displayed an inverse response-enhanced structural assembly upon illumination-revealing a novel mechanism for light-induced reinforcement that expands the array of photo-responsive materials.

These diverse behaviours establish a platform for designing stimulus-responsive delivery systems with programmable release profiles. The biocompatible nature of CD droplets, coupled with their ability to sequester both photoacids and anticancer drugs, positions them as particularly promising candidates for targeted cancer therapy applications.

CHAPTER 6: REFERENCES

1. Vaishnav, J. K.; Mukherjee, T. K. Highly Photostable and Two-Photon Active Quantum Dot-Polymer Multicolor Hybrid Coacervate Droplets. *Langmuir* **2019**, 35, 11764–11773.
2. Saini, B.; Singh, R. R.; Mukherjee, T. K. Biocompatible pH-Responsive Luminescent Coacervate Nanodroplets from Carbon Dots and Poly(diallyldimethylammonium chloride) toward Theranostic Applications. *ACS Appl. Nano Mater* **2020**, 3, 5826−5837.
3. Xing, Y.; Zeng, B.; Yang, W. Light responsive hydrogels for controlled drug delivery. *Frontiers in Bioengineering and Biotechnology,* **2022**, 10, 2296-4185.
4. Yucknovsky, A.; Amdursky, N. Photoacids and Photobases: Applications in Functional Dynamic Systems. *Angewandte Chemie*. **2025**, e202422963.
5. Lafon, S.; Martin, N. Reversible photocontrol of DNA coacervation. *Methods in Enzymology*. **2020**, 646, 329-351.
6. Williams, S. D.; Koga, S.; Kak, C. R. C.; Majreka, A.; Patil, J. A.; Maan, S.; Polymer/nucleotide droplets as bio-inspired functional micro-compartments. *Soft Matter*, **2012**, 8, 6004–6014.
7. Tian, B. H.; Fan, B.; Peng, X. J.; Luan, Z. K. A cleaner two-step synthesis of high purity diallyldimethylammonium chloride monomers for flocculant preparation. *Journal of environmental sciences (China).* **2005**, 17, 798–801.
8. Butler, G. B.; Angelo, R. J. Polymerization of Diallyldimethylammonium Chloride. *J. Am. Chem. Soc.* **1957**, 79, 3128–3131.
9. Liao, Y. Design and Applications of Metastable-State Photoacids. *Acc. Chem. Res.* **2017**, 50, 1956−1964.
10. Haberfield, P. Phototropic molecules. Phase Transfer as a Method for Detecting Transient Species. *J. Am. Chem. Soc.* **1987**, 109, 6177−6178.
11. Emond, M.; Le Saux, T.; Maurin, S.; Baudin, J.-B.; Plasson, R.; Jullien, L. 2-Hydroxyazobenzenes to Tailor pH Pulses and Oscillations with Light. *Chem. Eur. J.* **2010**, 16, 8822−8831.

12. Shi, Z.; Peng, P.; Strohecker, D.; Liao, Y. Long-Lived Photoacid Based upon a Photochromic Reaction. *J. Am. Chem. Soc.* **2011**, 133, 14699−14703.
13. Willson, C. G. Advances in Resist Technology. *Proc. SPIE*. **1984**, 469, 195−201.
14. Arnaut, L. G.; Formosinho, S. J. Excited-State Proton Transfer Reactions I. Fundamentals and Intermolecular Reactions. *Journal of Photochemistry and Photobiology, A.* **1993**, 75, 1−20.
15. Wan, P.; Shukla, D. Utility of Acid-Base Behaviour of Excited-States of Organic Molecules. *Chem. Rev*. **1993**, 93, 571−584.
16. Tolbert, L.; Solntsev, K. M. Excited-State Proton Transfer: From Constrained Systems to "Super" Photoacids to Superfast Proton Transfer. *Acc. Chem. Res*. **2002**, 35, 19−27.
17. Liao, Y. Design and Applications of Metastable-State Photoacids. *Acc. Chem. Res.* **2017**, 50, 1956−1964.
18. Ireland, J. F.; Wyatt, P. A. H. Acid-Base Properties of Electronically Excited States of Organic Molecules. *Adv. Phys. Org. Chem.* **1976**, 12, 131−221.
19. Forster, T. Primary photophysical processes. *Pure Appl. Chem.***1973**, 34, 225−234.
20. Liu, Y.; He, J.; Yang, K.; Yi, C.; Liu, Y.; Nie, L.; Khashab, N. M.; Chen, X.; Nie, Z. Folding Up of Gold Nanoparticle Strings into Plasmonic Vesicles for Enhanced Photoacoustic Imaging. *Angew.Chem., Int. Ed*. **2015**, 54, 15809−15812.
21. Uritski, A.; Huppert, D. Temperature dependence of solvation dynamics of probe molecules in methanol-doped ice and in liquid ethanol. *J. Phys. Chem. A* **2007**, 111, 10544−10551
22. Amoruso, G.; Taylor, V. C. A.; Duchi, M.; Goodband, E.; Oliver, T. A. A. Following Bimolecular Excited-State Proton Transfer between Hydroxycoumarin and Imidazole Derivatives. *J. Phys. Chem. B.* **2019**, 123, 4745−4756.
23. Shizuka, H. Excited-State Proton-Transfer Reactions and Proton-Induced Quenching of Aromatic Compounds. *Acc. Chem. Res*. **1985**, 18, 141−147.

24. Sritharan, S.; Sivalingam, N.; A comprehensive review on time-tested anticancer drug doxorubicin. *Life Sci.* **2021**, 278, 119527.
25. Simkovitch, R.; Kisin-Finfer, E.; Shomer, S.; Gepshtein, R.; Shabat, D.; Huppert, D. Ultrafast excited-state proton transfer from hydroxycoumarin-dipicolinium cyanine dyes. *Journal of Photochemistry and Photobiology a-Chemistry.* **2013**, 254, 45−53.
26. Discher, B. M.; Won, Y.-Y.; Ege, D. S.; Lee, J. C-M.; Bates, F. S.; Discher, D. E.; Hammer, D. A. Polymersomes: Tough Vesicles Made from Diblock Copolymers. *Science*. **1999**, 284, 1143−1146.
27. Yuk, H.; Lu, B.; Zhao, X. Hydrogel Bioelectronics. *Chem. Soc. Rev.* **2019**, 48, 1642−1667.
28. Yan, X.; Delgado, M.; Fu, A.; Alcouffe, P.; Gouin, S. G.; Fleury, E.; Katz, J. L.; Ganachaud, F.; Bernard, J. Simple but Precise Engineering of Functional Nanocapsules Through Nanoprecipitation. *Angew. Chem., Int. Ed.* **2014**, 53, 6910−6913.
29. Keating, C.D. Aqueous Phase Separation as a Possible Route to Compartmentalization of Biological Molecules. *Acc. Chem. Res*. **2012**, 45, 2114−2124.
30. Crosby, J.; Treadwell, T.; Hammerton, M.; Vasilakis, K.; Crump, M. P.; Williams, D. S.; Mann, S. Stabilization and Enhanced Reactivity of Actinorhodin Polyketide Synthase Minimal Complex in Polymer-Nucleotide Coacervate Droplets. *Chem. Commun*. **2012**, 48, 11832−11834.
31. Mason, A. F.; Buddingh, B. C.; Williams, D. S.; van Hest, J. C. M. Hierarchical Self-Assembly of a Copolymer-Stabilized Coacervate Protocell. *J. Am. Chem. Soc*. **2017**, 139, 17309−17312.
32. Drobot, B.; Iglesias-Artola, J. M.; Vay, K. L.; Mayr, V.; Kar, M.; Kreysing, M.; Mutschler, H.; Tang, T.-Y. D. Compartmentalised RNA Catalysis in Membrane-Free Coacervate Protocells. *Nat. Commun*. **2018**, 9, 3643.
33. Rivankar, Sangeeta. An overview of doxorubicin formulations in cancer therapy. *Journal of Cancer Research and Therapeutics.* **2014**, 10, 853-858.